

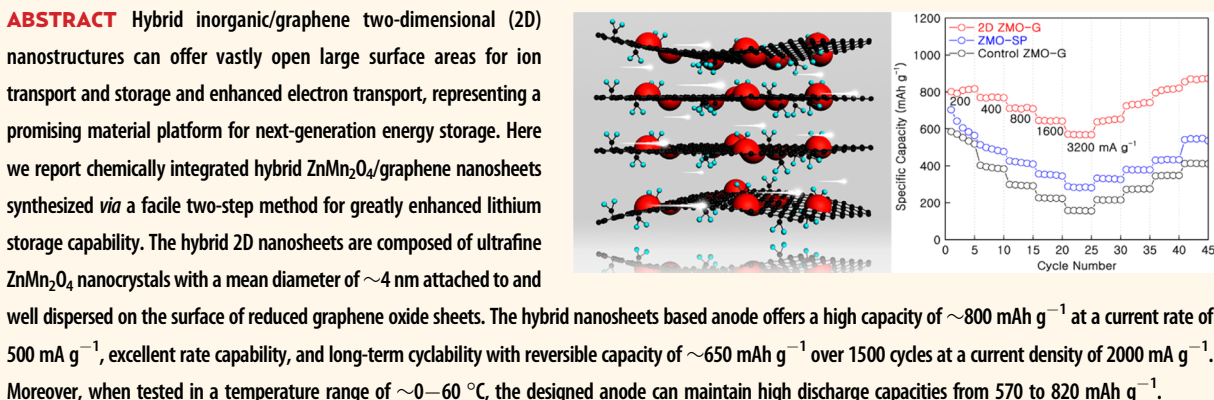
Chemically Integrated Two-Dimensional Hybrid Zinc Manganate/Graphene Nanosheets with Enhanced Lithium Storage Capability

Pan Xiong,^{†,‡,§} Borui Liu,^{†,§} Vincent Teran,[§] Yu Zhao,[†] Lele Peng,[†] Xin Wang,^{‡,*} and Guihua Yu^{†,*}

[†]Materials Science and Engineering Program and Department of Mechanical Engineering, The University of Texas at Austin, Austin, Texas 78712, United States,

[‡]Key Laboratory for Soft Chemistry and Functional Materials of Ministry of Education, Nanjing University of Science and Technology, Nanjing, China, and

[§]Department of Chemical Engineering, The University of Texas at Austin, Austin, Texas 78712, United States. ^{†,‡}P. Xiong and B. Liu contributed equally to this work.



KEYWORDS: two-dimensional nanosheets · ZnMn_2O_4 · mixed transitional-metal oxides · graphene · Li-ion battery · energy storage

Transition-metal oxides (TMOs), such as SnO_2 ,^{1,2} Co_3O_4 ,³ FeO_x ,^{1,4} and Mn_3O_4 ,⁵ have been widely studied as anode materials for rechargeable lithium-ion batteries (LIBs) owing to their potentially higher specific capacities than that of graphite. Unfortunately, these simple metal oxides exhibit low reversible capacity and poor rate capability. Recently, mixed transition-metal oxides (MTMOs, denoted as $\text{A}_x\text{B}_{3-x}\text{O}_4$; $\text{A}, \text{B} = \text{Co, Ni, Zn, Mn, Fe, etc.}$), which are the combinations of two TMOs or a TMO with a post-TMO, have been explored as attractive anode materials owing to their higher electronic conductivity and larger specific capacities than those of simple TMOs.^{6–8} One of the most attractive MTMO-based anode materials is ZnMn_2O_4 (ZMO), which shows high theoretical capacity (1008 mAh g^{-1} based on the first-time lithiation reaction $\text{ZnMn}_2\text{O}_4 + 9\text{Li}^+ + 9\text{e}^- \rightarrow \text{ZnLi} + 2\text{Mn} + 4\text{Li}_2\text{O}$; 784 mAh g^{-1} based on the reaction $\text{ZnLi} + 2\text{Mn} + 3\text{Li}_2\text{O} \leftrightarrow \text{ZnO} + 2\text{MnO} + 7\text{Li}^+ + 7\text{e}^-$), natural abundance, environmental

friendliness, and favorable operation voltage compared to the Co- or Fe-based oxides.⁹ However, ZMO material suffers from low electronic/ionic conductivity and detrimental structural collapse upon lithiation/delithiation. Rational design and synthesis of ZMO nanostructures^{10–13} have been proven to be an effective approach to alleviate intractable problems.¹⁴ However, intrinsically poor electronic/ionic conductivities of ZMO have yet to be well resolved.

Designing hybrid carbon–MTMO nanostructures is another appealing strategy to solve the aforementioned challenges to improve the reaction kinetics and realize superior energy storage performances.^{15,16} Among the various carbon nanomaterials, graphene has been a leading candidate for a variety of advanced nanostructures with superior performance due to its superlative electronic properties, large surface area, and excellent flexibility and chemical compatibility, as manifested by extensive studies.^{17–19} Up to now, a few graphene–MTMO anode

* Address correspondence to
ghyu@austin.utexas.edu;
wangx@mail.njust.edu.cn.

Received for review June 20, 2014
and accepted July 29, 2014.

Published online July 29, 2014
10.1021/nn5041203

© 2014 American Chemical Society

materials, such as CoFe_2O_4 –graphene composites²⁰ and graphene-wrapped ZnMn_2O_4 ,²¹ have been prepared by the self-assembly method or electrostatic interaction strategy. However, due to a possibly weak interaction between graphene and MTMO nanocrystals, the performances still need to improve. Thus, controlled synthesis of MTMO–graphene with an integrated nanostructure is extremely desirable. For many graphene–inorganic nanoparticle hybrids reported in the literature, a general two-step synthesis is of particular interest and significance to form hybrid nanostructures with potentially strong coupling between nanoparticles and graphene substrates.^{5,22} It is believed that intimate interactions between graphene and inorganic nanoparticles can not only enhance effective and rapid charge transfer⁵ but also prevent volume expansion/contraction and aggregation of nanoparticles upon cycling.² Moreover, the dispersed nanoparticles anchored on graphene sheets can provide a large surface area for Li-ion (Li^+) access and effectively shorten the diffusion pathway for Li^+ transport.^{3,23} Therefore, hybrid nanostructures based on ZMO nanocrystals and graphene sheets can synergize the advantageous features above and are thus expected to achieve greatly improved lithium storage capability.

Here we report a facile two-step synthesis approach involving a polyol process followed by thermal annealing for growing well-distributed ZMO nanocrystals on reduced graphene oxide (rGO) sheets to form a 2D ZnMn_2O_4 –graphene (2D ZMO–G) nanostructure (Figure 1), where ZMO nanoparticles with a mean diameter of $\sim 4\text{--}5$ nm are uniformly anchored on graphene nanosheets. Due to the unique 2D nanosheet structure with ultrafine ZMO nanocrystals, the resulting 2D ZMO–G hybrid electrode exhibits a high specific capacity of ~ 650 mAh g⁻¹ over 1500 cycles at 2000 mA g⁻¹, as well as high rate capability and cycling stability.

RESULTS AND DISCUSSION

The 2D ZMO–G nanosheet samples were synthesized via the following two steps (see Supporting Information for more details). First, ZMO precursors were mixed in ethylene glycol with GO nanosheets, which were then partially reduced to rGO during solution synthesis.^{24,25} Subsequently, thermal treatment was performed to transform ZMO precursors to ZMO nanocrystals, yielding the designed 2D hybrid ZMO–G nanosheets. Conductive graphene sheets act as flexible 2D substrates for uniform anchoring of ZMO nanoparticles. On one hand, the graphene sheets in the 2D ZMO–G hybrid can provide an elastic buffer space to accommodate volume expansion/contraction of ZMO nanoparticles during charge/discharge processes, while preventing the aggregation of ZMO nanoparticles upon cycling, thus potentially leading to good cycling stability. On the other hand, the graphene sheets have good electric conductivity and

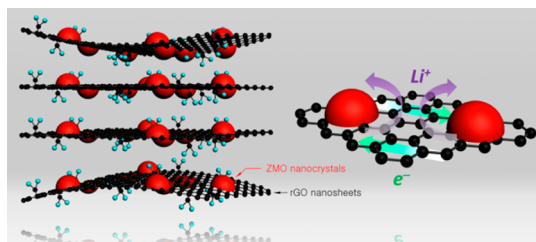


Figure 1. Schematic illustration of the 2D hybrid ZMO–G nanostructure and synergistic electrochemical characteristics of the 2D hybrid nanosheets.

can serve as electron conduction channels for ZMO nanoparticles, facilitating effective charge transport favorable for high rate performance.^{5,26} Moreover, unique 2D hybrid nanostructures can enable large electrochemically active sites for Li^+ transport for higher specific capacity.^{23,27}

The structural characterization on the hybrid ZMO–G nanosheets was first carried out using scanning electron microscopy (SEM) and scanning transmission electron microscope (STEM). As clearly shown in Figure 2a,b, rGO nanosheets were uniformly loaded with ultrafine ZMO nanoparticles, which have an average particle size of ~ 4 nm with a standard deviation of $\sim 8\%$, evidenced by the corresponding size distribution analysis (inset of Figure 2b). Since Li^+ diffusion strongly depends on the transport length and accessible sites of the active materials,³ the ultrafine ZMO nanoparticles could not only expose more electrochemically active sites for Li^+ shuttling in/out of active hosts compared to bulk ZMO but also shorten the diffusion pathways for Li^+ transport, which may contribute to high rate performance. A high-resolution transmission electron microscope (HRTEM) image (Figure 2c) showed that the crystalline near-spherical ZMO nanoparticles were well distributed on the surface of rGO sheets, and no obvious aggregates were observed. The clear lattice fringes of ~ 0.49 nm corresponded well to the (101) plane of ZMO. In addition, even after a lengthy sonication during the preparation of the TEM specimen, the ZMO nanocrystals were still immobilized on the surface of the rGO sheets, suggesting strong interactions between ZMO nanoparticles and rGO.^{22,23,28}

The chemical identity of these nanoparticles was further analyzed by X-ray diffraction (XRD) and elemental mapping. XRD analysis of the 2D ZMO–G hybrid (Figure 2d) indicated crystalline ZMO nanoparticles with a tetragonal phase (JCPDS card no. 24-1133). A broad peak at around 25° could be attributed to the (002) plane of disorderly stacked graphene sheets (Figure S1).²⁹ No typical diffraction peaks of GO (Figure S1) were observable in the XRD pattern of the 2D hybrid, which is in agreement with the GO being fully exfoliated and partially reduced to rGO during the synthesis process.^{24,25} The presence of Zn, Mn, O, and C elements in 2D ZMO–G was confirmed by elemental mapping

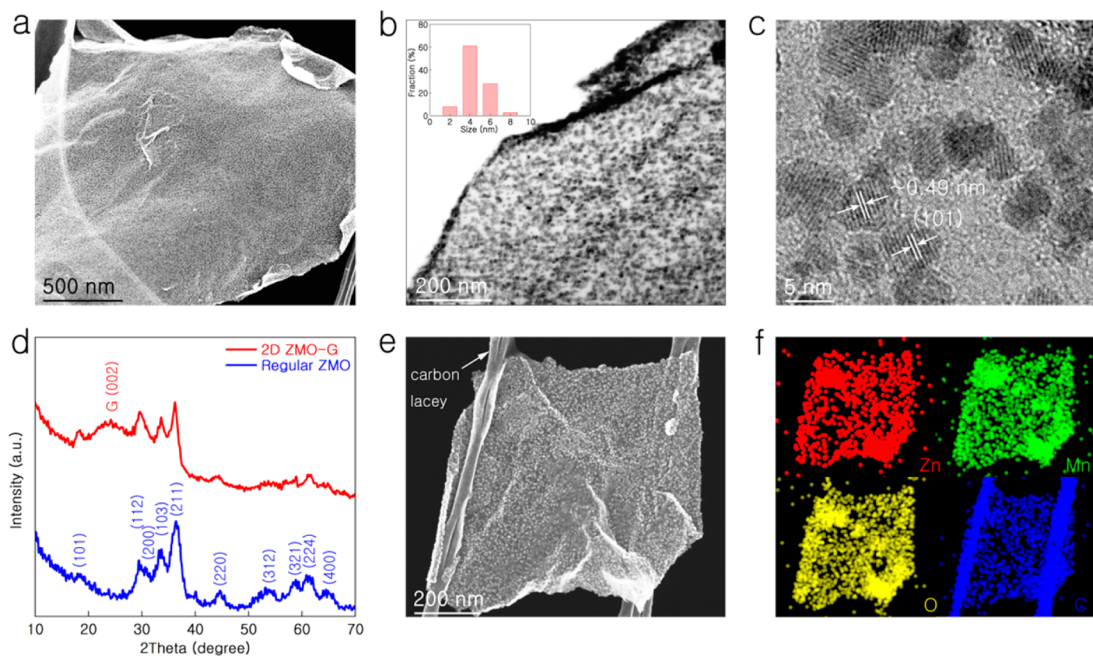


Figure 2. (a) Scanning electron microscopy (SEM) image of 2D ZMO–G hybrid nanosheets. (b) Scanning transmission electron microscope (STEM) image of 2D ZMO–G. Inset: Corresponding particle size distribution of the ZMO nanocrystals. (c) High-resolution TEM image of 2D ZMO–G. (d) X-ray diffraction (XRD) patterns of regular ZMO and 2D ZMO–G. (e, f) STEM image and corresponding elemental mapping images of Zn, Mn, O, and C.

analysis (Figure 2e and f), in which the uniform distribution of Zn, Mn, O, and C was experimentally mapped out. Raman scattering, which indicates the vibrational modes of both crystalline and amorphous materials, could provide complementary structural information to the XRD analysis. Raman spectra of 2D ZMO–G (Figure S2) showed five peaks at 321, 375, 667, 1367, and 1593 cm^{-1} , respectively. The peaks at 1367 and 1593 cm^{-1} are attributed to the D and G bands of rGO, respectively.⁴ The three peaks below 1000 cm^{-1} correspond to the spinel ZnMn_2O_4 phase, which are in good agreement with the previous reports.³⁰ The mass ratio of ZMO:G in 2D ZMO–G was determined by thermal gravimetric analysis (TGA) to be close to 3:1 (Figure S3). The measured Brunauer–Emmett–Teller (BET) showed 2D ZMO–G had a high surface area of $119\text{ m}^2\text{ g}^{-1}$, much higher than reported ZMO hollow microspheres ($28\text{ m}^2\text{ g}^{-1}$).¹² An adsorption–desorption isotherm exhibited a type IV hysteresis loop (Figure S4), which is characteristic of a mesoporous material with different pore sizes. The formation of ZMO nanoparticles grown on rGO sheets may be attributed to chemical interactions between the ZMO and the oxygen functional group sites in the GO domains.^{22,23,28} During thermal annealing, due to strong chemical interactions, the ZMO nanoparticles on rGO nanosheets showed little aggregation or migration.^{23,28} Such a process could be confirmed by control experiments, in which only bulk agglomerates composed of ZMO nanoparticles were produced (Figure S5) under the same synthesis conditions in the absence of GO.

The electrochemical characteristics of 2D ZMO–G hybrid nanosheets were first examined by electrochemical

impedance spectroscopy (EIS) (Figure 3a and Figure S6). The diameter of semicircle in the higher frequency region is attributed to the charge transfer resistance related to the reaction between the active material and electrolyte interface. 2D ZMO–G hybrid nanosheets based electrodes (note that no carbon additives are needed for electrodes) exhibited the smallest charge transfer resistance (24 ohm) compared to control ZMO–G (157 ohm) (ZMO physically mixed with rGO) and ZMO–SP (66 ohm) (ZMO physically mixed with Super-P carbon). In contrast to physically mixed samples, the chemically integrated 2D ZMO–G hybrid leads to a much more effective charge transfer process, resulting in lower charge transfer resistance.^{5,23,26} Figure 3b presents cyclic voltammogram tests of 2D ZMO–G hybrid based electrodes at a scan rate of 0.1 mV s^{-1} . In the first cycle, there were two peaks at around 1.1 and 0.8 V, which were attributed to the reduction of Mn^{3+} to Mn^{2+} and formation of a solid electrolyte interphase (SEI), respectively.^{11,31} The cathodic peak at 0.41 V was due to the reduction reactions of Zn^{2+} and Mn^{2+} to metallic nanodomains of Zn^0 and Mn^0 embedded in the Li_2O matrix and a Zn–Li alloying reaction.^{12,13} In the first anodic sweep, the broad peak at around 0.6 V was attributed to a Zn–Li dealloying reaction,³² while the two broad peaks at 1.18 and 1.45 V were attributed to oxidation reactions of Mn^0 to Mn^{2+} and Zn^0 to Zn^{2+} , respectively. In the subsequent cycles, the peak disappeared at around 0.8 V, indicating the good stability of the formed SEI layer. The reduction peaks of Zn^{2+} and Mn^{2+} to their metallic states were shifted to 0.54 and 0.52 V, respectively, which could be

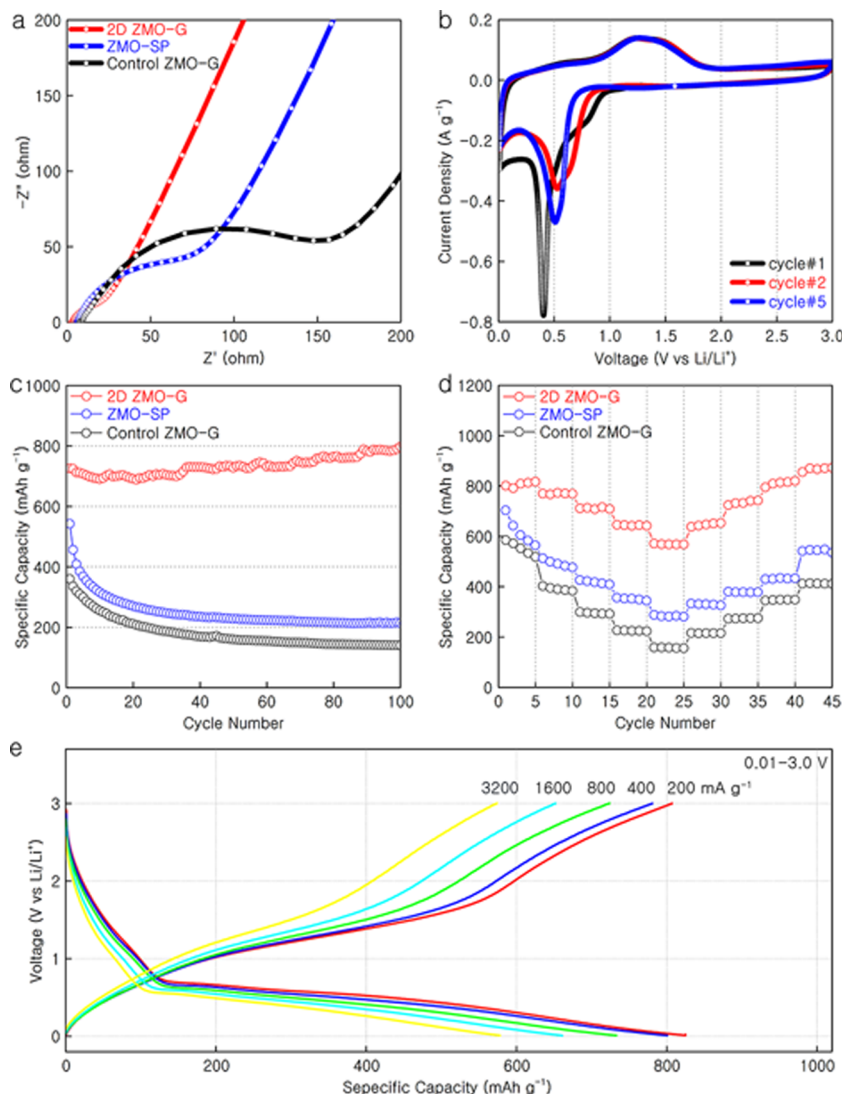


Figure 3. (a) Electrochemical impedance spectroscopy (EIS) of 2D ZMO-G, control ZMO-G, and ZMO-SP electrodes. (b) Cyclic voltammograms of 2D ZMO-G at a sweep rate of 0.1 mV s^{-1} . (c) Cycling performance of 2D ZMO-G, control ZMO-G, and ZMO-SP electrodes at a current density of 500 mA g^{-1} . (d) Rate performance of three different electrodes at various current densities of $200, 400, 800, 1600$, and 3200 mA g^{-1} . (e) Charge/discharge curves of a 2D ZMO-G electrode at various current densities.

associated with structural rearrangement.¹⁰ The similar phenomenon had been observed in some reported ZMO anodes.^{11–13} A lower polarization of the 2D ZMO-G hybrid anode was observed compared to the previous ZMO anodes,^{10–13} which may be attributed to the improved conductivity (Figure 3a) and shortened Li⁺ diffusion pathway gained by the unique hybrid nanosheet structure in ZMO-G electrodes (Figure 2b).

To further evaluate the electrochemical characteristics of the 2D ZMO-G hybrid based anode, stability tests were carried out at a current rate of 500 mA g^{-1} for 100 cycles. Figure 3c shows that reversible specific capacities of *ca.* 730 and *ca.* 800 mAh g^{-1} (all specific capacities estimated based on total mass of electrodes) were obtained at the first cycle and after 100 cycles, respectively. The capacity retention after 100 charge/discharge cycles was greater than 100%. It is believed

that the escalation in capacity is likely due to the activation process as well as the significant structural and electrochemical reinforcements of graphene in the composite electrode.^{33,34} The control ZMO-G and ZMO-SP electrodes, by contrast, show specific capacities of only *ca.* 360 and *ca.* 540 mAh g^{-1} at the first cycle, respectively, and specific capacities further decreased to 140 and 210 mAh g^{-1} after 100 charge/discharge cycles, resulting in a capacity retention of 38.8% and 39.5%, respectively. The substantially higher reversible capacity of 2D ZMO-G is attributed to the large electrochemically active surface area and shortened Li⁺ diffusion pathways resulting from the 2D open nanostructures.^{3,5,23} Moreover, unique 2D hybrid nanostructures could maintain structural integrity upon cycling through synergistic enhancement between ultrafine ZMO nanoparticles and flexible graphene sheets,^{23,35}

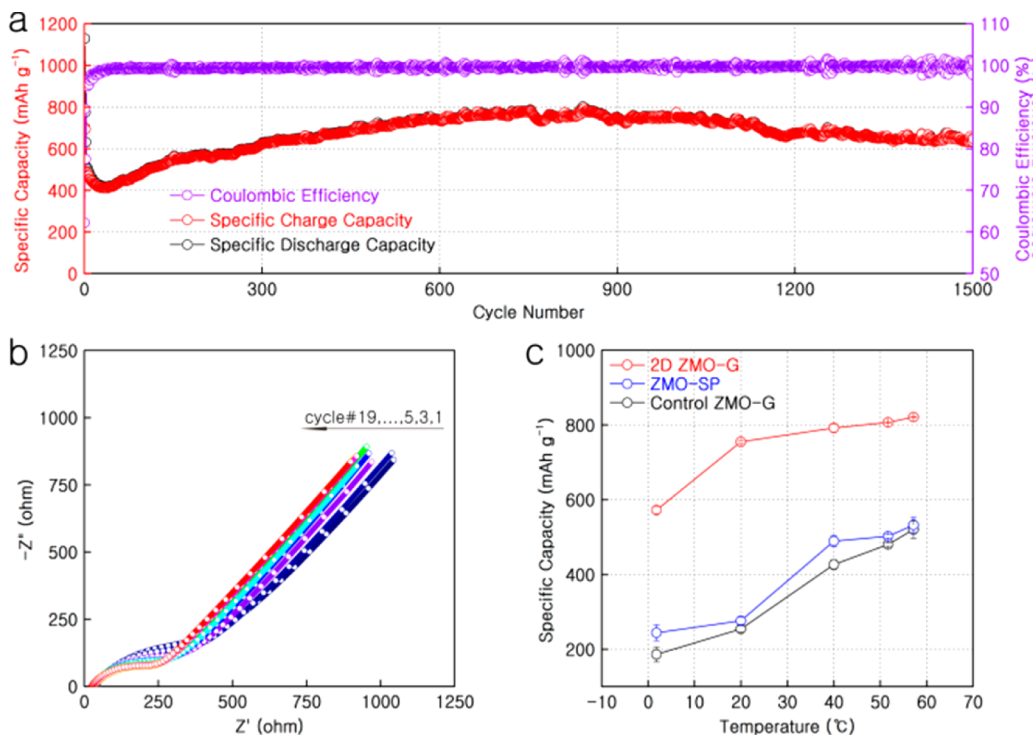


Figure 4. (a) Cycling performance and Coulombic efficiency of a 2D ZMO–G hybrid electrode at a current rate of 2000 mA g⁻¹ for more than 1500 cycles. (b) EIS profiles of a 2D ZMO–G electrode at different cycles. (c) Temperature-dependent discharge capacity of three different electrodes at a current density of 500 mA g⁻¹: 2D ZMO–G, control ZMO–G, and ZMO–SP.

thus leading to good cycling stability. As shown in Figure S7, the structure integrity of 2D ZMO–G was well preserved even after 1500 cycles. The rate performance of 2D ZMO–G is shown in Figure 3d, where a stable specific capacity of *ca.* 806 mAh g⁻¹ (Figure 3e) was obtained at a low current density of 200 mA g⁻¹. Even at a high current density of 3200 mA g⁻¹, the reversible capacity was still maintained as high as *ca.* 568 mAh g⁻¹ (Figure 3e) with a 71% capacity retention. However, for control ZMO–G and ZMO–SP, only *~*30% and *~*50% capacity retentions were obtained, respectively, as current density increased from 200 to 3200 mA g⁻¹. Notably, the rate performance of this 2D ZMO–G is superior compared to the previously reported ZMO anodes and recent graphene-wrapped ZnMn₂O₄ nanorods^{10–13,21} (Table S1) and among the best reported transition-metal oxide based anode materials (including Mn₃O₄, Co₃O₄, ZnCo₂O₄, NiCo₂O₄, and CoMn₂O₄) with high rate capability.^{3,5,6,36,37}

The long-term cyclability measurement of the 2D ZMO–G hybrid anode was performed at a current rate of 2000 mA g⁻¹ for more than 1500 deep charge/discharge cycles (Figure 4a). A specific capacity of *~*800 mAh g⁻¹ was obtained at the first cycle, and the capacity slightly decreased in the first 50 cycles and gradually increased to *ca.* 800 mAh g⁻¹ during the following few hundred cycles. This phenomenon is consistent with previous reports and could be attributed to electrochemical activation of anode materials³³ and heterogeneous storage of Li at the developing

nanodomain and/or nanophase interfaces with extensive interfacial areas.^{34,38,39} After 1500 cycles, a stable discharge capacity of *~*650 mAh g⁻¹ could still be obtained, resulting in a capacity retention of *~*81%. The cycling stability of our 2D ZMO–G hybrid anode is significantly better than the previously reported ZMO-based anodes (Table S1). Such a high cycling stability of an MTMO-based anode has rarely been reported so far. The Coulombic efficiency of the first cycle was 63%, which then promptly increased to 95% within four cycles and afterward stabilized over 99.5% for the subsequent cycles. In order to confirm the formation of a stable SEI layer, cell impedance measurements were carried out. The EIS plots of a 2D ZMO–G hybrid anode obtained at the end of cycles 1, 3, and 5 to 19 subsequent to the initial lithiation/delithiation are shown in Figure 4b. Compared with the EIS spectrum of a fresh cell (Figure 3a), the increase in impedance of 2D ZMO–G was presumably due to the formation of an SEI in the first few cycles, and no obvious further impedance increase was observed.

In addition, since key electrochemical characteristics of LIBs such as the Li⁺ diffusion coefficient are essentially temperature dependent,⁴⁰ the ability to sustain efficient battery operations over a wide temperature range is important. To this end, we evaluated the temperature-dependent specific discharge capacities at a current density of 500 mA g⁻¹ at various operation temperatures, as shown in Figure 4c. Multiple data points were taken at different temperatures conducted

for each sample. The 2D ZMO–G hybrid electrode exhibited a high specific capacity of *ca.* 820 mAh g^{−1} at 57.2 °C. More importantly, a specific capacity of *ca.* 570 mAh g^{−1} (only \sim 30% capacity decrease) can still be delivered even under low temperatures, down to 1.8 °C. In contrast, the specific capacities of control ZMO–G and ZMO–SP were sharply decreased by \sim 64% and 54% over the same temperature range from 1.8 to 57.2 °C, respectively.

The outstanding electrochemical characteristics of 2D ZMO–G hybrid nanosheets are largely attributed to the chemically integrated 2D nanosheet structure. Owing to the covalent anchoring of ZMO on a graphene substrate, charge carriers could be effectively and rapidly transferred between ZMO and the current collector through the highly conductive graphene, leading to high electric/ionic conductivities.^{3,5} The unique 2D nanosheet and ultrafine ZMO nanoparticles not only provided a high surface area for Li storage but also shortened the diffusion pathways for Li⁺ shuttling in/out of the active host matrix, beneficial for the high reversible capacity.^{3,5,23,26} Furthermore, the

unique 2D nanosheet maintained structural integrity upon cycling,^{23,27} since the ultrafine ZMO nanoparticles could accommodate the internally anisotropic stresses and volume changes induced by Li alloying/dealloying processes, resulting in a relatively stable SEI layer.^{35,41,42} The flexible graphene sheets accommodated the volume expansion/contraction of ZMO nanoparticles and prevented the aggregation of ZMO nanoparticles during electrochemical cycling, which are responsible for the high rate capability and cycling stability.^{3,5,23,26}

CONCLUSIONS

In summary, we have designed and synthesized a chemically integrated 2D hybrid ZnMn₂O₄/graphene nanosheet structure through a facile two-step approach. By synergizing advantageous features of this unique 2D hybrid nanostructure, ZnMn₂O₄/graphene hybrid based electrodes exhibit large specific capacity, high rate capability, and excellent cycling performance, indicating its potential as a promising candidate material for a high-performance, inexpensive, and environmentally friendly anode for lithium-ion batteries.

MATERIALS AND METHODS

Synthesis of 2D ZMO–G Hybrid Nanosheets. GO is prepared from purified natural graphite by a modified Hummers method. A typical experiment for the synthesis of 2D ZMO–G is as follows: 6 mg of graphite oxide powder is dispersed into 15 mL of ethylene glycol with sonication for 2 h; 0.1 mmol of Zn(Ac)₂·2H₂O and 0.2 mmol of Mn(Ac)₂·2H₂O are dissolved in 5 mL of ethylene glycol. The above two systems are then mixed together and stirred for 60 min. The obtained solution is transferred into a round-bottom flask and heated to 170 °C in an oil bath. After refluxing for 120 min, the solution is cooled to room temperature naturally, and the precipitate is collected by centrifugation and washed with ethanol several times. The precipitate is then annealed at 200 °C in air for 2 h with a heating rate of 0.5 °C min^{−1} to get the 2D ZMO–G. To prepare regular ZMO, 0.1 mmol of Zn(Ac)₂·2H₂O, 0.2 mmol of Mn(Ac)₂·2H₂O, and 20 mL of ethylene glycol were used for the reaction, like the typical synthesis mentioned above. The rGO was prepared by the same method without Zn(Ac)₂·2H₂O and Mn(Ac)₂·2H₂O.

Characterizations. The structure of the as-synthesized samples was characterized by powder XRD patterns performed on a Philips diffractometer. The morphology of the samples was investigated using SEM, STEM (Hitachi S5500), and TEM (JEOL JEM-2100F). The TG analysis was performed by a TGA/SDTA851e thermogravimetric analyzer under standard atmosphere from 25 to 850 °C at a heating rate of 10 °C min^{−1}. Nitrogen sorption isotherms and BET surface area were measured with an automated gas sorption analyzer (AutoSorb iQ2, Quantachrome Instruments). Raman spectra were obtained on a Renishaw Raman system.

Electrochemical Measurements. A mixture consisting of 90 wt % 2D ZMO–G and 10 wt % binding agent (polyvinylidene difluoride) was milled with *N*-methylpyrrolidone to form a homogeneous slurry, which was then coated onto a copper foil. For comparison, the ZMO physically mixed with rGO (or Super P carbon) in the weight ratio of 75:25 (the same weight ratio as the rGO in 2D ZMO–G) was also used as the active materials, named control ZMO–G and ZMO–SP, respectively. The as-prepared electrodes were dried under vacuum at 110 °C for 10 h. After being pressed sealed, the electrodes were assembled into coin cells (CR2032) in an argon-filled glovebox using 1 mol L^{−1} LiPF₆ in ethylenecarbonate and diethylenecarbonate (1:1, v/v) as the electrolyte and Li metal as the counter electrode. The average mass loading of all

electrodes is \sim 0.8–1 mg cm^{−2}. The assembled coin cells were tested in the voltage range 0.01–3.0 V on a BioLogic Instrument (BioLogic VMP-3 model). A criterion temperature benchtop (ESPEC BTZ-133) was adopted to provide a constant-temperature environment for the temperature-dependent tests. In order for the cell to reach a thermal equilibrium before testing, the cell was kept for 24 h at each temperature.

Conflict of Interest: The authors declare no competing financial interest.

Supporting Information Available: Experimental details, XRD patterns, TGA analysis, SEM and TEM images, additional EIS spectra, and electrochemical characterizations. This material is available free of charge via the Internet at <http://pubs.acs.org>.

Acknowledgment. We thank Prof. John B. Goodenough, Prof. Arumugam Manthiram, and Prof. Joseph H. Koo at the University of Texas at Austin for instrumental support and valuable discussions. G.Y. acknowledges the financial support of the startup grant from the University of Texas at Austin and from the Welch Foundation grant F-1861. P.X. and X.W. acknowledge the financial support from NSAF (No. U1230125) and the Graduate School of Nanjing University of Science and Technology.

REFERENCES AND NOTES

- Poizot, P.; Laruelle, S.; Gruegeon, S.; Dupont, L.; Tarascon, J. M. Nano-Sized Transition-Metal Oxides as Negative-Electrode Materials for Lithium-Ion Batteries. *Nature* **2000**, *407*, 496–499.
- Paek, S.-M.; Yoo, E.; Honma, I. Enhanced Cyclic Performance and Lithium Storage Capacity of SnO₂/Graphene Nanoporous Electrodes with Three-Dimensionally Delaminated Flexible Structure. *Nano Lett.* **2008**, *9*, 72–75.
- Wu, Z.-S.; Ren, W.; Wen, L.; Gao, L.; Zhao, J.; Chen, Z.; Zhou, G.; Li, F.; Cheng, H.-M. Graphene Anchored with Co₃O₄ Nanoparticles as Anode of Lithium Ion Batteries with Enhanced Reversible Capacity and Cyclic Performance. *ACS Nano* **2010**, *4*, 3187–3194.
- Zhou, G.; Wang, D.-W.; Li, F.; Zhang, L.; Li, N.; Wu, Z.-S.; Wen, L.; Lu, G. Q.; Cheng, H.-M. Graphene-Wrapped Fe₃O₄ Anode Material with Improved Reversible Capacity and

Cyclic Stability for Lithium Ion Batteries. *Chem. Mater.* **2010**, *22*, 5306–5313.

- Wang, H.; Cui, L.-F.; Yang, Y.; Sanchez Casalongue, H.; Robinson, J. T.; Liang, Y.; Cui, Y.; Dai, H. Mn_3O_4 -Graphene Hybrid as a High-Capacity Anode Material for Lithium Ion Batteries. *J. Am. Chem. Soc.* **2010**, *132*, 13978–13980.
- Liu, B.; Zhang, J.; Wang, X.; Chen, G.; Chen, D.; Zhou, C.; Shen, G. Hierarchical Three-Dimensional $ZnCo_2O_4$ Nanowire Arrays/Carbon Cloth Anodes for a Novel Class of High-Performance Flexible Lithium-Ion Batteries. *Nano Lett.* **2012**, *12*, 3005–3011.
- Yuan, C.; Wu, H. B.; Xie, Y.; Lou, X. W. Mixed Transition-Metal Oxides: Design, Synthesis, and Energy-Related Applications. *Angew. Chem., Int. Ed.* **2014**, *53*, 1488–1504.
- Zou, F.; Hu, X.; Sun, Y.; Luo, W.; Xia, F.; Qie, L.; Jiang, Y.; Huang, Y. Microwave-Induced *in Situ* Synthesis of Zn_2GeO_4 /N-Doped Graphene Nanocomposites and Their Lithium-Storage Properties. *Chem.—Eur. J.* **2013**, *19*, 6027–6033.
- Yang, Y.; Zhao, Y.; Xiao, L.; Zhang, L. Nanocrystalline $ZnMn_2O_4$ as a Novel Lithium-Storage Material. *Electrochem. Commun.* **2008**, *10*, 1117–1120.
- Xiao, L.; Yang, Y.; Yin, J.; Li, Q.; Zhang, L. Low Temperature Synthesis of Flower-like $ZnMn_2O_4$ Superstructures with Enhanced Electrochemical Lithium Storage. *J. Power Sources* **2009**, *194*, 1089–1093.
- Bai, Z.; Fan, N.; Sun, C.; Ju, Z.; Guo, C.; Yang, J.; Qian, Y. Facile Synthesis of Loaf-like $ZnMn_2O_4$ Nanorods and Their Excellent Performance in Li-Ion Batteries. *Nanoscale* **2013**, *5*, 2442–2447.
- Zhou, L.; Wu, H. B.; Zhu, T.; Lou, X. W. Facile Preparation of $ZnMn_2O_4$ Hollow Microspheres as High-Capacity Anodes for Lithium-Ion Batteries. *J. Mater. Chem.* **2012**, *22*, 827–829.
- Zhang, G.; Yu, L.; Wu, H. B.; Hoster, H. E.; Lou, X. W. Formation of $ZnMn_2O_4$ Ball-in-Ball Hollow Microspheres as a High-Performance Anode for Lithium-Ion Batteries. *Adv. Mater.* **2012**, *24*, 4609–4613.
- Levi, M. D.; Aurbach, D. Diffusion Coefficients of Lithium Ions during Intercalation into Graphite Derived from the Simultaneous Measurements and Modeling of Electrochemical Impedance and Potentiostatic Intermittent Titration Characteristics of Thin Graphite Electrodes. *J. Phys. Chem. B* **1997**, *101*, 4641–4647.
- Sun, Y.; Hu, X.; Luo, W.; Xia, F.; Huang, Y. Reconstruction of Conformal Nanoscale MnO on Graphene as a High-Capacity and Long-Life Anode Material for Lithium Ion Batteries. *Adv. Funct. Mater.* **2013**, *23*, 2436–2444.
- Shin, W. H.; Jeong, H. M.; Kim, B. G.; Kang, J. K.; Choi, J. W. Nitrogen-Doped Multiwall Carbon Nanotubes for Lithium Storage with Extremely High Capacity. *Nano Lett.* **2012**, *12*, 2283–2288.
- Geim, A. K.; Novoselov, K. S. The Rise of Graphene. *Nat. Mater.* **2007**, *6*, 183–191.
- Geim, A. K. Graphene: Status and Prospects. *Science* **2009**, *324*, 1530–1534.
- Yang, X.; Cheng, C.; Wang, Y.; Qiu, L.; Li, D. Liquid-Mediated Dense Integration of Graphene Materials for Compact Capacitive Energy Storage. *Science* **2013**, *341*, 534–537.
- Liu, S.; Xie, J.; Fang, C.; Cao, G.; Zhu, T.; Zhao, X. Self-Assembly of a $CoFe_2O_4$ /Graphene Sandwich by a Controllable and General Route: Towards a High-Performance Anode for Li-Ion Batteries. *J. Mater. Chem.* **2012**, *22*, 19738–19743.
- Zheng, Z.; Cheng, Y.; Yan, X.; Wang, R.; Zhang, P. Enhanced Electrochemical Properties of Graphene-Wrapped $ZnMn_2O_4$ Nanorods for Lithium-Ion Batteries. *J. Mater. Chem. A* **2014**, *2*, 149–154.
- Liang, Y.; Li, Y.; Wang, H.; Zhou, J.; Wang, J.; Regier, T.; Dai, H. Co_3O_4 Nanocrystals on Graphene as a Synergistic Catalyst for Oxygen Reduction Reaction. *Nat. Mater.* **2011**, *10*, 780–786.
- Li, W.; Wang, F.; Feng, S.; Wang, J.; Sun, Z.; Li, B.; Li, Y.; Yang, J.; Elzatahry, A. A.; Xia, Y.; et al. Sol–Gel Design Strategy for Ultradispersed TiO_2 Nanoparticles on Graphene for High-Performance Lithium Ion Batteries. *J. Am. Chem. Soc.* **2013**, *135*, 18300–18303.
- Nethravathi, C.; Rajamathi, M. Chemically Modified Graphene Sheets Produced by the Solvothermal Reduction of Colloidal Dispersions of Graphite Oxide. *Carbon* **2008**, *46*, 1994–1998.
- Xu, C.; Wang, X.; Zhu, J. Graphene–Metal Particle Nanocomposites. *J. Phys. Chem. C* **2008**, *112*, 19841–19845.
- Wang, H.; Yang, Y.; Liang, Y.; Cui, L.-F.; Sanchez Casalongue, H.; Li, Y.; Hong, G.; Cui, Y.; Dai, H. $LiMn_{1-x}Fe_xPO_4$ Nanorods Grown on Graphene Sheets for Ultrahigh-Rate-Performance Lithium Ion Batteries. *Angew. Chem., Int. Ed.* **2011**, *123*, 7502–7506.
- Yang, S.; Feng, X.; Wang, L.; Tang, K.; Maier, J.; Müllen, K. Graphene-Based Nanosheets with a Sandwich Structure. *Angew. Chem., Int. Ed.* **2010**, *49*, 4795–4799.
- Wang, H.; Dai, H. Strongly Coupled Inorganic–Nanocarbon Hybrid Materials for Energy Storage. *Chem. Soc. Rev.* **2013**, *42*, 3088–3113.
- Chen, H.; Müller, M. B.; Gilmore, K. J.; Wallace, G. G.; Li, D. Mechanically Strong, Electrically Conductive, and Biocompatible Graphene Paper. *Adv. Mater.* **2008**, *20*, 3557–3561.
- Kim, J. G.; Lee, S. H.; Kim, Y.; Kim, W. B. Fabrication of Free-Standing $ZnMn_2O_4$ Mesoscale Tubular Arrays for Lithium-Ion Anodes with Highly Reversible Lithium Storage Properties. *ACS Appl. Mater. Interfaces* **2013**, *5*, 11321–11328.
- Cao, Y.; Xiao, L.; Ai, X.; Yang, H. Surface-Modified Graphite as an Improved Intercalating Anode for Lithium-Ion Batteries. *Electrochem. Solid-State Lett.* **2003**, *6*, A30–A33.
- Wang, J.; King, P.; Huggins, R. A. Investigations of Binary Lithium-Zinc, Lithium-Cadmium and Lithium-Lead Alloys as Negative Electrodes in Organic Solvent-Based Electrolyte. *Solid State Ionics* **1986**, *20*, 185–189.
- Wu, H.; Yu, G.; Pan, L.; Liu, N.; McDowell, M. T.; Bao, Z.; Cui, Y. Stable Li-Ion Battery Anodes by *in-Situ* Polymerization of Conducting Hydrogel to Conformally Coat Silicon Nanoparticles. *Nat. Commun.* **2013**, *4*, 1943.
- Peng, C.; Chen, B.; Qin, Y.; Yang, S.; Li, C.; Zuo, Y.; Liu, S.; Yang, J. Facile Ultrasonic Synthesis of CoO Quantum Dot/Graphene Nanosheet Composites with High Lithium Storage Capacity. *ACS Nano* **2012**, *6*, 1074–1081.
- Song, T.; Xia, J.; Lee, J.-H.; Lee, D. H.; Kwon, M.-S.; Choi, J.-M.; Wu, J.; Doo, S. K.; Chang, H.; Park, W. I.; et al. Arrays of Sealed Silicon Nanotubes as Anodes for Lithium Ion Batteries. *Nano Lett.* **2010**, *10*, 1710–1716.
- Li, J.; Xiong, S.; Liu, Y.; Ju, Z.; Qian, Y. High Electrochemical Performance of Monodisperse $NiCo_2O_4$ Mesoporous Microspheres as an Anode Material for Li-Ion Batteries. *ACS Appl. Mater. Interfaces* **2013**, *5*, 981–988.
- Zhou, L.; Zhao, D.; Lou, X. W. Double-Shelled $CoMn_2O_4$ Hollow Microcubes as High-Capacity Anodes for Lithium-Ion Batteries. *Adv. Mater.* **2012**, *24*, 745–748.
- Maier, J. Nanoionics: Ion Transport and Electrochemical Storage in Confined Systems. *Nat. Mater.* **2005**, *4*, 805–815.
- Courtel, F. M.; Duncan, H.; Abu-Lebdeh, Y.; Davidson, I. J. High Capacity Anode Materials for Li-Ion Batteries Based on Spinel Metal Oxides AMn_2O_4 (A = Co, Ni, and Zn). *J. Mater. Chem.* **2011**, *21*, 10206–10218.
- Ramadesigan, V.; Northrop, P. W. C.; De, S.; Santhanagopalan, S.; Braatz, R. D.; Subramanian, V. R. Modeling and Simulation of Lithium-Ion Batteries from a Systems Engineering Perspective. *J. Electrochem. Soc.* **2012**, *159*, R31–R45.
- Lee, S. W.; McDowell, M. T.; Berla, L. A.; Nix, W. D.; Cui, Y. Fracture of Crystalline Silicon Nanopillars during Electrochemical Lithium Insertion. *Proc. Natl. Acad. Sci.* **2012**, *109*, 4080–4085.
- Ebner, M.; Marone, F.; Stampaconi, M.; Wood, V. Visualization and Quantification of Electrochemical and Mechanical Degradation in Li Ion Batteries. *Science* **2013**, *342*, 716–720.